Journal of Nuclear Medicine, published on June 13, 2024 as doi:10.2967/jnumed.124.267469

Synthesis of ^{64}Cu-, ^{55}Co-, and ^{68}Ga-Labeled Radiopharmaceuticals Targeting Neurotensin Receptor-1 for Theranostics: Adjusting In Vivo Distribution Using Multiamine Macrocycles

German O. Fonseca Cabrera*[1], Xinrui Ma*[1,2], Wilson Lin*[3], Tao Zhang[1], Weiling Zhao[1], Liqin Pan[1], Xiaomei Li[4], Todd E. Barnhart[3], Eduardo Aluicio-Sarduy[3], Huaifu Deng[1], Xuedan Wu[1], Kadalipura P. Rakesh[1], Zibo Li[1], Jonathan W. Engle[2], and Zhanhong Wu[1]

[1]*Biomedical Research Imaging Center, Department of Radiology, UNC Lineberger Comprehensive Cancer Center, University of North Carolina at Chapel Hill, Chapel Hill, North Carolina;* [2]*Joint Department of Biomedical Engineering, University of North Carolina at Chapel Hill and North Carolina State University, Chapel Hill, North Carolina;* [3]*Department of Medical Physics, University of Wisconsin, Madison, Wisconsin; and* [4]*Accunovo Biotechnologies, Inc., Chapel Hill, North Carolina*

The development of theranostic radiotracers relies on their binding to specific molecular markers of a particular disease and the use of corresponding radiopharmaceutical pairs thereafter. This study reports the use of multiamine macrocyclic moieties (MAs), as linkers or chelators, in tracers targeting the neurotensin receptor-1 (NTSR-1). The goal is to achieve elevated tumor uptake, minimal background interference, and prolonged tumor retention in NTSR-1–positive tumors. **Methods:** We synthesized a series of neurotensin antagonists bearing MA linkers and metal chelators. The MA unit is hypothesized to establish a strong interaction with the cell membrane, and the addition of a second chelator may enhance water solubility, consequently reducing liver uptake. Small-animal PET/CT imaging of [^{64}Cu]Cu-DOTA-SR-3MA, [^{64}Cu]Cu-NT-CB-NOTA, [^{68}Ga]Ga-NT-CB-NOTA, [^{64}Cu]Cu-NT-CB-DOTA, and [^{64}Cu]Cu-NT-Sarcage was acquired at 1, 4, 24, and 48 h after injection using H1299 tumor models. [^{55}Co]Co-NT-CB-NOTA was also tested in HT29 (high NTSR-1 expression) and Caco2 (low NTSR-1 expression) colorectal adenocarcinoma tumor models. Saturation binding assay and internalization of [^{55}Co]Co-NT-CB-NOTA were used to test tracer specificity and internalization in HT29 cells. **Results:** In vivo PET imaging with [^{64}Cu]Cu-NT-CB-NOTA, [^{68}Ga]Ga-NT-CB-NOTA, and [^{55}Co]Co-NT-CB-NOTA revealed high tumor uptake, high tumor-to-background contrast, and sustained tumor retention (≤48 h after injection) in NTSR-1–positive tumors. Tumor uptake of [^{64}Cu]Cu-NT-CB-NOTA remained at 76.9% at 48 h after injection compared with uptake 1 h after injection in H1299 tumor models, and [^{55}Co]Co-NT-CB-NOTA was retained at 60.2% at 24 h compared with uptake 1 h after injection in HT29 tumor models. [^{64}Cu]Cu-NT-Sarcage also showed high tumor uptake with low background and high tumor retention 48 h after injection **Conclusion:** Tumor uptake and pharmacokinetic properties of NTSR-1–targeting radiopharmaceuticals were greatly improved when attached with different nitrogen-containing macrocyclic moieties. The study results suggest that NT-CB-NOTA labeled with either ^{64}Cu/^{67}Cu, ^{55}Co/^{58m}Co, or ^{68}Ga (effect of ^{177}Lu in tumor to be determined in future studies) and NT-Sarcage labeled with ^{64}Cu/^{67}Cu or ^{55}Co/^{58m}Co may be excellent diagnostic and therapeutic radiopharmaceuticals targeting NTSR-1–positive cancers. Also, the introduction of MA units to other ligands is warranted in future studies to test the generality of this approach.

Key Words: radiotheranostic agent; prostate cancer; PET; neurotensin receptor; ^{64}Cu; ^{55}Co; ^{68}Ga

J Nucl Med 2024; 00:1–7
DOI: 10.2967/jnumed.124.267469

Prostate cancer is the most frequently diagnosed noncutaneous malignancy and the second leading cause of cancer-related death among men in the United States (*1*). Although several treatments exist, there is a need for significantly improved prostate cancer management (*2,3*). Indeed, a new targeted radionuclide therapy has been developed for advanced prostate cancer patients by targeting prostate-specific membrane antigen (PSMA) (*4*). In 2022, [^{177}Lu]Lu-PSMA-617 (Pluvicto; Novartis) received U.S. Food and Drug Administration approval for prostate cancer treatment (*5,6*). Despite this progress, a proportion of prostate cancer patients exhibit inherent resistance to this therapy (*7,8*). It has been estimated that up to 30% of patients may not respond effectively to PSMA-based radionuclide therapy (*9–12*). Furthermore, acquired resistance to PSMA-based radionuclide therapy can also occur over time. Cancer cells may adapt and develop mechanisms to evade therapy effects. Resistance might arise because of various mechanisms, such as alterations in PSMA expression or changes in DNA repair mechanisms. There is a necessity to develop new therapeutic and prognostic methods for the management of advanced-stage prostate cancer. Although multiple factors may contribute to prostate cancer development, progression, and resistance to therapy, increasing evidence suggests that intraprostate neuroendocrinelike cells play an important role in androgen-independent recurrent prostate cancer (*13–17*). Prostate cancer may even become enriched in (or entirely composed of) neuroendocrine cell clusters after long-term antiandrogen therapy. Secreted by neuroendocrinelike prostate cells, neurotensin has numerous physiologic effects predominantly mediated through its high-affinity receptor, neurotensin receptor-1 (NTSR-1), which is expressed and activated in aggressive prostate cancer cells

Received Jan. 22, 2024; revision accepted May 7, 2024.
For correspondence or reprints, contact Zibo Li (ziboli@med.unc.edu), Jonathan W. Engle (jwengle@wisc.edu), or Zhanhong Wu (zhanhong_wu@med.unc.edu).
*Contributed equally to this work.
Published online Jun. 13, 2024.

but not in normal prostate epithelial cells (*17–19*). In advanced prostate cancer, NTSR-1 is recruited as an alternative growth pathway in the absence of androgens (*20–22*). Thus, NTSR-1–targeted radiopharmaceuticals hold great potential as novel treatments for the management of NTSR-1–positive prostate cancer. Moreover, NTSR-1 has been found to be overexpressed in a large portion of lung, breast, pancreatic, and colorectal cancers, all of which can also benefit from NTSR-1–targeted agents.

With the ability to see what we treat and treat what we see, radiotheranostic agents can be screened quickly using an imaging radionuclide and subsequently used for treatment once the isotope is changed to a matched therapeutic radionuclide. For example, tracers labeled with positron-emitting radionuclides (β^+) are used for diagnosis and patient screening by PET, whereas the same agent labeled with ionizing particle–emitting radionuclides (emitters of β-particles [β^-], α-particles, or Auger electrons) can be used for therapy purposes (*23*). Although ^{68}Ga/^{177}Lu is a widely used theranostic pair, their half-lives do not match, and the use of 2 different elements may increase the chance of pharmacokinetic discrepancy. A true theranostic pair involves the use of same-element radioisotopes for both imaging and therapy. Two of such matched pairs are ^{64}Cu (PET isotope for imaging, half-life = 12.7 h, I_{β^+} = 18%, $<E_{\beta^+}>$ = 280 keV)/^{67}Cu (β-emitter for therapy, half-life = 62 h, I_{β^-} = 100%, $<E_{\beta^-}>$ = 141 keV) and ^{55}Co (PET isotope, half-life = 17.5 h, I_{β^+} = 77%, $<E_{\beta^+}>$ = 570 keV)/^{58m}Co (Auger electron emitter for therapy, half-life = 9.1 h, 100% internal conversion). Metal-binding chelators such as bicyclic Sarcage (1-*N*-(4-aminobenzyl)-3,6,10,13,16,19-hexaazabicyclo[6.6.6]-eicosane-1,8-diamine), NOTA, and DOTA readily form stable complexes in vivo with both copper and cobalt cations (*24–26*).

To develop NTSR-1–targeted radiotheranostic agents, an appropriate ligand must be used. NTSR-1 is activated by the endogenous 13-amino-acid peptide agonist neurotensin and the hexapeptide neuromedin N (section 12 of the supplemental materials; supplemental materials are available at http://jnm.snmjournals.org). The C-terminal hexapeptide portion of neurotensin, NT8-13, represents the binding epitope and contains all determinants for NTSR-1 activation (*27*). Initial NTSR-1–targeted radiopharmaceuticals were focused on stabilized peptide agonists, which were labeled with ^{18}F, ^{11}C, ^{68}Ga, and ^{64}Cu and showed high-contrast imaging of NTSR-1–positive tumor models (*28,29*). However, fast clearance profiles and moderate tumor uptake values made these peptides unsuitable for targeted radionuclide therapy. Nonpeptidic antagonists (Fig. 1A) represent another category of NTSR-1 ligands, which were labeled with ^{18}F and ^{68}Ga for PET imaging and ^{177}Lu for therapy applications (*28,29*). For example, Schulz et al. evaluated 3BP-227 for ^{177}Lu radiotherapy of colon carcinoma in a preclinical study in 2017 (*30*), and Baum et al. initiated a radiotherapy trial on patients with metastatic or locally advanced NTSR-1–expressing cancers with promising results (*31*). Tracer ^{225}Ac-FPI-2059 is currently in preclinical development for the treatment of solid tumors expressing NTSR-1 (*32,33*). Previously, we developed SR142948A-related derivatives and found that those attached to chelators based on 1,4,8,11-tetraazabicyclo[6.6.2]hexadecane (CB)-cyclam (Fig. 1B) can greatly reduce the background uptake and enhance tumor retention of ^{64}Cu-labeled agents compared with [^{64}Cu]Cu-3BP-227. Liver was the only major organ that showed uptake of the NTSR-1–targeted agents (*34*).

In this report, we developed NTSR-1–targeted constructs with the potential for ^{64}Cu/^{67}Cu, ^{55}Co/^{58m}Co, and ^{68}Ga/^{177}Lu labeling. PET imaging with ^{64}Cu, ^{55}Co, and ^{68}Ga was used to study in vivo

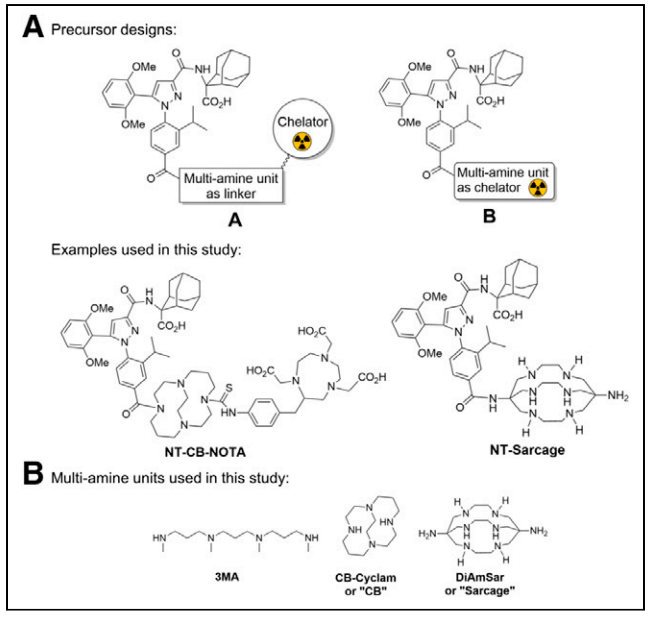

FIGURE 1. (A) Precursor designs and examples that illustrate rational design. (B) Multiamine units used in this study.

radiotracer distribution. To synthesize agents with improved tumor uptake, improved tumor-to-background ratios, and extended tumor residence time, we hypothesized that the net charge around the tracer is a key factor in determining how a tracer interacts with its receptor and other cell substructures such as the cell membrane. Thus, we used a synthetic antagonistic NTSR-1–targeting ligand, and charge modification was performed by introducing structural changes at the linker and chelator moieties of the tracer (Fig. 1A). Multiamine macrocyclic moieties (MAs) affect the distribution of SR142948A derivatives (*28,29,35*), possibly by enhancing the linkage with the negatively charged external surface of the cell membrane, through ionic interactions, with the MAs' positively charged basic nitrogens (section 5 of the supplemental materials) (*36*). This would increase the tracer concentration and the time the tracer spends near its receptor. MAs may also improve the target-to-background ratio of tracers by modifying their pharmacokinetic properties. Furthermore, MAs such as CB-cyclam and Sarcage are rigid macrocycles with several nitrogen atoms capable of establishing additional hydrogen bonding to water molecules, which makes the tracer more hydrophilic and helps minimize undesired liver uptake.

MATERIALS AND METHODS

Small-Animal PET/CT Imaging and Biodistribution of [^{64}Cu]Cu-DOTA-SR-3MA, [^{64}Cu]Cu-NT-CB-NOTA, [^{68}Ga]Ga-NT-CB-NOTA, [^{64}Cu]Cu-NT-CB-DOTA, and [^{64}Cu]Cu-NT-Sarcage

All animal studies were conducted under a protocol approved by the Institutional Animal Care and Use Committee of the University of North Carolina at Chapel Hill. Female nude mice (nu/nu immunodeficient, 5–6 wk old) were obtained from the Animal Facility at University of North Carolina at Chapel Hill. Approximately 5 million H1299 cells in a 1:1 mixture of Matrigel (BD Biosciences) and phosphate-buffered saline were injected subcutaneously into the left or right shoulder and leg to establish the tumor xenograft. Animals were ready for imaging studies after the tumor reached a volume of 200 mm^3.

For PET/CT imaging, each mouse (n = 3) was injected with 3–6 MBq of [^{64}Cu]Cu-DOTA-SR-3MA. The same settings were applied to the

PET images acquired with [^{64}Cu]Cu-NT-CB-NOTA, [^{64}Cu]Cu-NT-CB-DOTA, and [^{64}Cu]Cu-NT-Sarcage. PET imaging acquired pharmacokinetic profiles at 1, 4, 24, and 48 h after injection. CT scans were acquired before PET imaging for anatomic reference. Mice were awakened between tracer injection and imaging times. Images were acquired with the PET/CT imaging system SuperArgus 4R (Sedecal Inc.). List-mode data were collected and reconstructed using the algorithm described before (*37*). Regions of interest were drawn using AMIDE software (Amide's a Medical Image Data Examiner). Organ uptake was expressed as mean ± SD of percentage injected dose per gram and corrected for radioactivity decay.

Small-Animal PET/CT Imaging and Biodistribution of [^{55}Co]Co-NT-CB-NOTA

All animal studies were conducted under a protocol approved by the University of Wisconsin Institutional Animal Care and Use Committee. Female athymic nude mice (5–6 wk old) were purchased from Jackson Laboratory. HT29 and Caco2 tumor inoculation, in vivo PET imaging, and ex vivo biodistribution were performed following methods reported by Lin et al. (*38*). Each mouse (n = 4) received 2.1 MBq of [^{55}Co]Co-NT-CB-NOTA. PET imaging acquired pharmacokinetic profiles at 1, 4, 9, and 24 h after injection. Ex vivo biodistribution studies were performed immediately after the 24-h PET scan to validate the in vivo PET imaging results.

The supplemental materials provide the synthetic schemes and protocols for new compounds and radiotracers (sections 2 and 3); radiolabeling details (section 4); saturation binding assay and internalization of [^{55}Co]Co-NT-CB-NOTA results (section 6); quantification of organ uptake and tumor-to-muscle ratios and comparison of tumor uptake, residence half-life, and tumor-to-muscle ratios between tracers (sections 7–9); and statistical analysis (section 10) (*39,40*).

RESULTS

Synthesis and In Vivo Biodistribution of Precursor DOTA-SR-3MA

First, we synthesized intermediate SR-3MA-NH (**2**) from the phenyl-Br (**1**) (*41*), and then it was conjugated to a DOTA chelator to obtain precursor DOTA-SR-3MA (**3**). Compound **3** has an additional nitrogen center compared with 3BP-227 (section 2.1 of the supplemental materials). After **3** was labeled with ^{64}Cu, in vivo PET imaging results showed high tumor uptake for [^{64}Cu]Cu-DOTA-SR-3MA (in H1299-tumor–bearing nu/nu mice) with relatively low background except for moderate uptake in the liver (Fig. 2). The linker homologation with the presence of an extra nitrogen atom seemed to have a positive impact on the in vivo PET imaging biodistribution, but the tumor uptake was moderately reduced. A more dramatic change in the MA structure was needed to reduce undesired liver uptake.

Synthesis and In Vivo Biodistribution of NT-CB–Based Precursors

Next, we explored whether the more rigid structure of macrocycle CB-cyclam could be used as an MA to improve the tumor-to-liver ratio obtained with **3.** NT-CB (**5**) was obtained in high yield from the corresponding precursor **1,** via its phenyl-carboxylic acid (**4**) derivative (section 2.2 of the supplemental materials). Next, precursors NT-CB-CA (**7**), NT-CB-Sarcage (**8**), NT-CB-NOTA (**9**), and NT-CB-DOTA (**10**) were easily synthesized in good yield (section 2.3 of the supplemental materials). Two additional precursors, NT-CB-succinimide-NOTA (**11**) and NT-CB-succinimide-DOTA (**12**), were successfully synthesized from **5,** but they were not tested for their in vivo PET imaging biodistribution during this study (section 2.4 of the supplemental materials). Next, we performed the ^{64}Cu labeling and in vivo PET imaging of **7** and **8.** [^{64}Cu]Cu-NT-CB-CA and [^{64}Cu]Cu-NT-CB-Sarcage both showed relatively low tumor uptake in our pilot PET imaging studies. We then focused our efforts on testing the biodistribution of **9** and **10.** Gratifyingly, in vivo PET imaging results with [^{64}Cu]Cu-NT-CB-NOTA, [^{68}Ga]Ga-NT-CB-NOTA (both in H1299-tumor–bearing mice), and [^{55}Co]Co-NT-CB-NOTA (in HT29-tumor–bearing mice) revealed high tumor uptake with low background and sustained tumor retention for up to 48 h after injection (Figs. 3–5, respectively). The presence of the CB-NOTA moiety in the tracer structure clearly improved the ratio of the tumor-to-background signal compared with [^{64}Cu]Cu-DOTA-SR-3MA. Unexpectedly, chemical replacement of the NOTA chelator with its DOTA analog and subsequent ^{64}Cu labeling to generate [^{64}Cu]Cu-NT-CB-DOTA did not provide the same level of improvement in H1299-tumor–bearing mice. Tumor uptake levels were similar to those of the NOTA analog; however, higher liver and kidney radiosignals were detected (Fig. 6). This might be caused by the in vivo stability limitation of the Cu-DOTA complex. This agent is worth further investigation given its α-particle therapy applications.

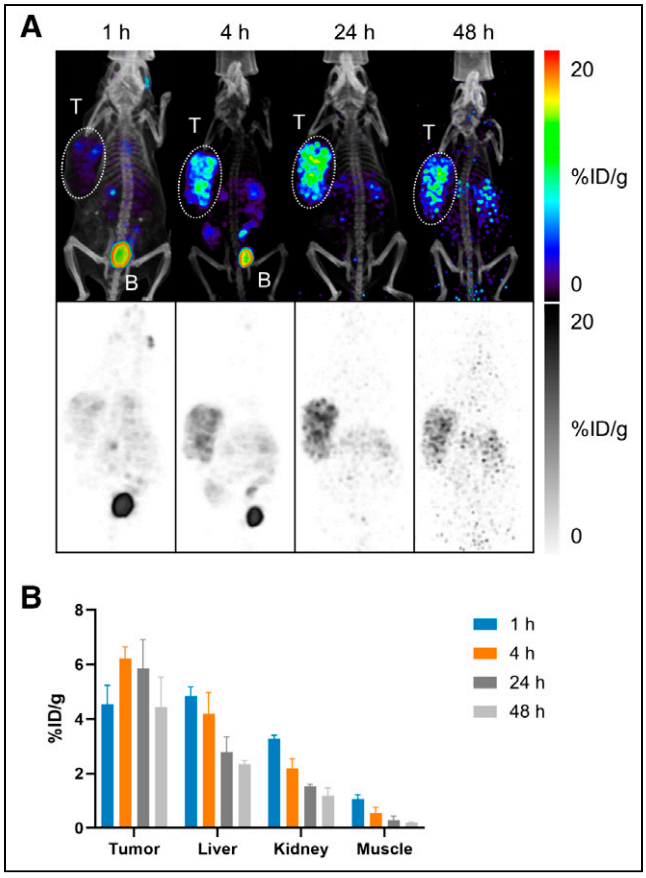

FIGURE 2. (A) Three-dimensional PET/CT images of [^{64}Cu]Cu-DOTA-SR-3MA in H1299-tumor–bearing nu/nu mice at 1, 4, 24, and 48 h after injection. (B) In vivo biodistribution analysis of approximately 4.5 MBq of [^{64}Cu]Cu-DOTA-SR-3MA at 1, 4, 24, and 48 h after injection (via tail vein). B = bladder; %ID/g = percentage injected dose per gram; T = tumor.

Synthesis and In Vivo Biodistribution of NT-Sarcage

Given the unexpected imaging result obtained with **8** and to remove any negative chemical interaction between Sarcage and other linkers present in the tracer, we decided to modify this precursor and synthesize an agent in which the neurotensin ligand

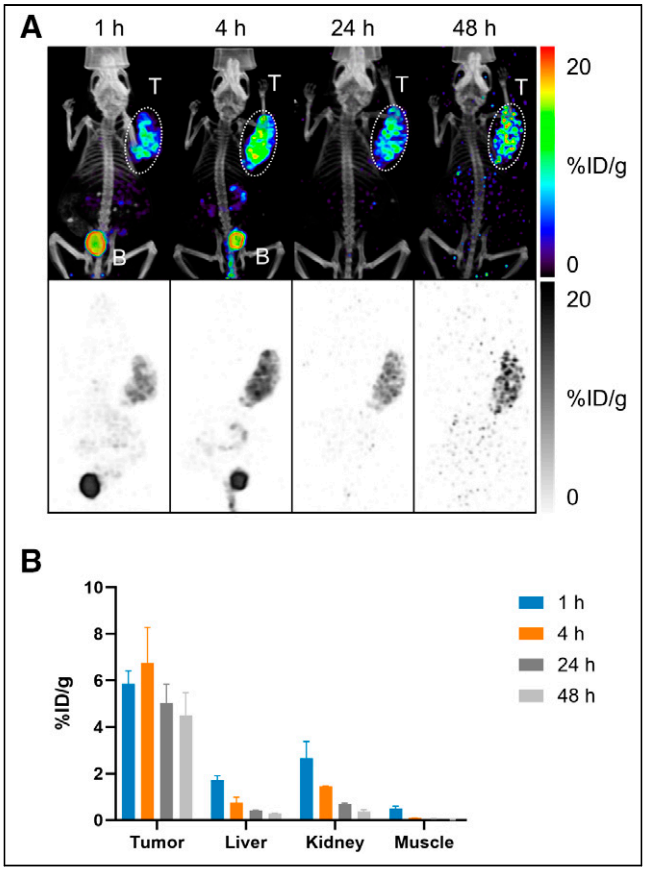

FIGURE 3. (A) In vivo biodistribution experiments showing 3-dimensional PET/CT images of [^{64}Cu]Cu-NT-CB-NOTA in H1299-tumor–bearing nu/nu mice at 1, 4, 24, and 48 h after injection. (B) Quantitative analysis of [^{64}Cu]Cu-NT-CB-NOTA in H1299-tumor–bearing mice at 1, 4, 24, and 48 h after injection. B = bladder; %ID/g = percentage injected dose per gram; T = tumor.

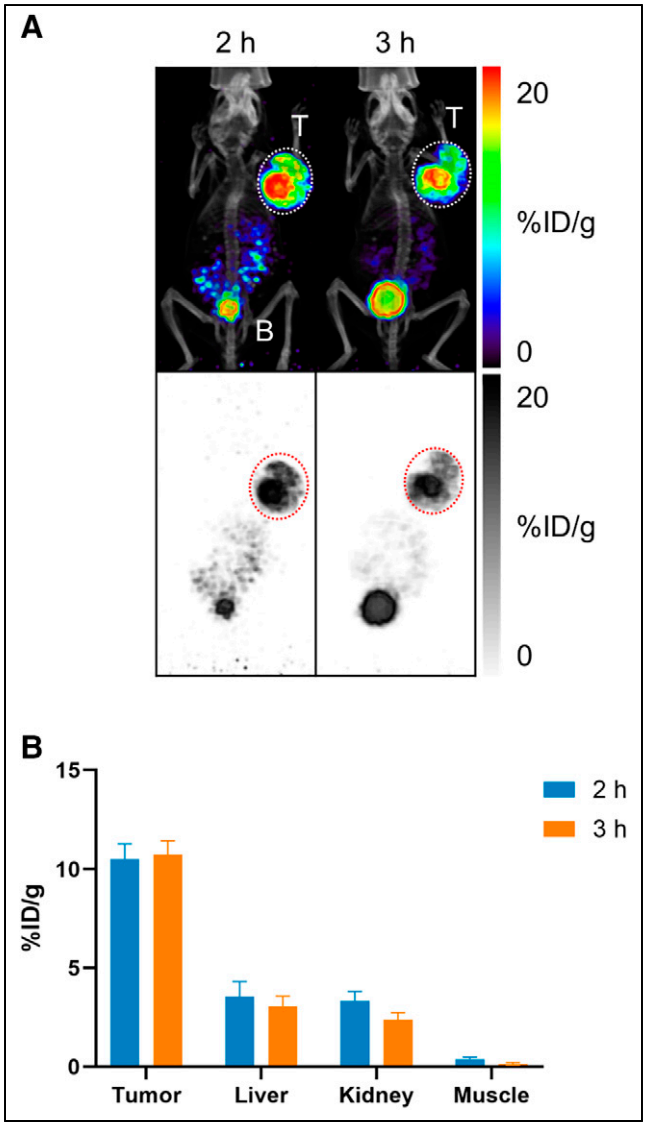

FIGURE 4. (A) Three-dimensional PET/CT images of [^{68}Ga]Ga-NT-CB-NOTA in H1299-tumor–bearing nu/nu mice at 2 and 3 h after injection. (B) Quantitative analysis of [^{68}Ga]Ga-NT-CB-NOTA in H1299-tumor–bearing mice at 2 and 3 h after injection. B = bladder; %ID/g = percentage injected dose per gram; T = tumor.

and the Sarcage chelator were directly connected, without any linker present between. NT-Sarcage (**6**) was then synthesized in one pot with a large yield from **4** (section 2.2 of the supplemental materials). The Sarcage moiety is directly attached through an amide functional group to the neurotensin ligand. With **6** in hand, we performed in vivo PET imaging studies of [^{64}Cu]Cu-NT-Sarcage in H1299-tumor–bearing mice (Fig. 7). [^{64}Cu]Cu-NT-Sarcage showed high tumor uptake with low background and high tumor retention at 48 h after injection. Initial labeling with Co also revealed interesting results (*42*). Remarkably, **6** can be modified further to add a second ligand to the cage. In this regard, a PSMA ligand (Lys-Glu-urea or *N*-[[[(1*S*)-5-amino-1-carboxypentyl]amino]carbonyl]-L-glutamic acid (**13**)) was linked to **6,** which may serve as a dual-targeting agent to address tumor heterogeneity limitations (**16a** and **16b**; section 2.5 of the supplemental materials). Detailed biologic evaluations of NT-Sarcage-PSMA compounds **16a** and **16b** as well as NT-CB–based precursors **11** and **12** will be performed in follow-up studies.

Tracer-Specific Binding to NTSR-1

We validated that the high tumor uptake was due to the specific binding of [^{64}Cu]Cu-NT-CB-NOTA to NTSR-1 by performing in vivo blocking experiments. The experiments were conducted by injecting a 100-fold molar excess of unlabeled neurotensin peptide (blocking agent) before the radioactive tracer in H1299-tumor–bearing nu/nu mice (section 11 of the supplemental materials). Also, the different tumor uptake of [^{55}Co]Co-NT-CB-NOTA between HT29 (high NTSR-1 expression) and Caco2 (low NTSR-1 expression) tumor models suggested specificity of the tracer for NTSR-1 (Fig. 5). Furthermore, the [^{55}Co]Co-NT-CB-NOTA cell surface binding and internalization potentials were tested in NTSR-1–positive HT29 cells. The binding saturation assays determined a dissociation constant of 3 ± 2 nM and an NTSR-1 density of $(0.7 \pm 0.2) \times 10^5$ per HT29 cell using a one-site binding model (section 6 of the supplemental materials; Supplemental Fig. 7A). [^{55}Co]Co-NT-CB-NOTA internalization reached a calculated plateau of 34% ± 2% cell-associated activity and a monoexponential internalization rate of $(1.7 \pm 0.3) \times 10^{-2}$ min^{-1} (section 6 of the supplemental materials; Supplemental Fig. 7B).

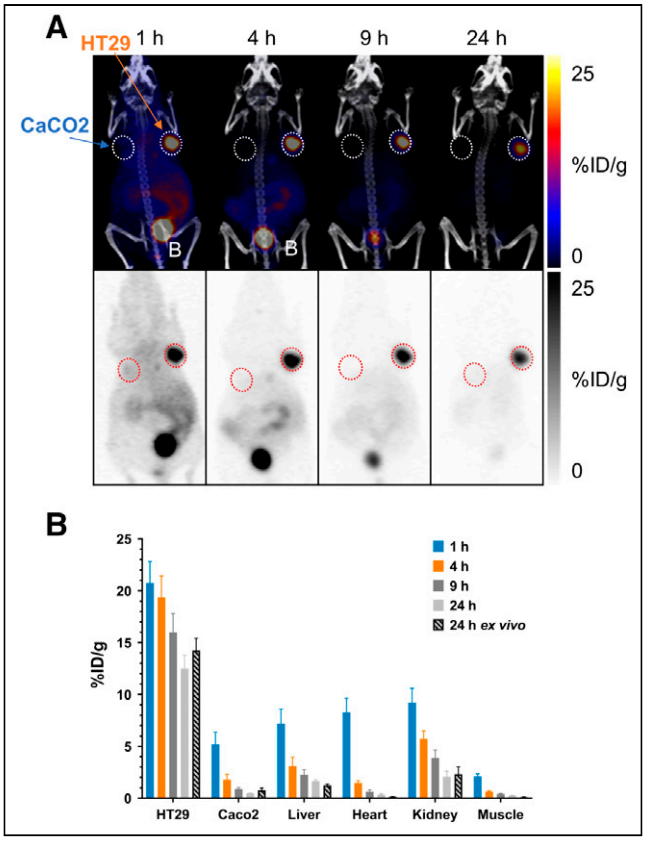

FIGURE 5. (A) Three-dimensional PET/CT images of [^{55}Co]Co-NT-CB-NOTA in HT29-tumor–bearing mice at 1, 4, 9, and 24 h after injection. Caco2 tumor is shown on left shoulder; HT29 tumor is shown on right shoulder. (B) Quantitative analysis of [^{55}Co]Co-NT-CB-NOTA in HT29-tumor–bearing mice at 1, 4, 9, 24, and 24 h ex vivo after injection. B = bladder; %ID/g = percentage injected dose per gram; T = tumor.

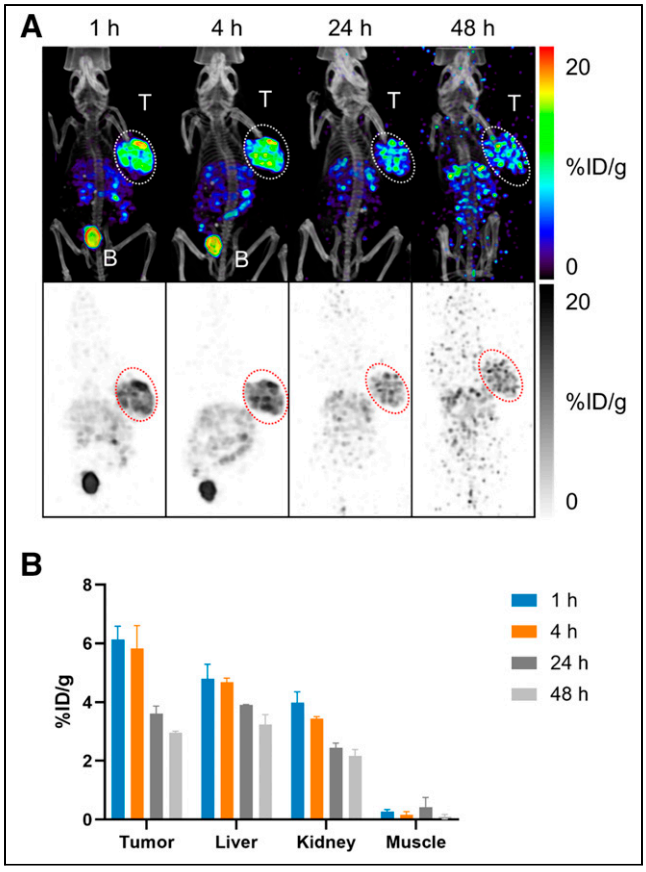

FIGURE 6. (A) Three-dimensional PET/CT representative images of [^{64}Cu]Cu-NT-CB-DOTA in H1299-tumor–bearing mice at 1, 4, 24, and 48 h after injection. (B) Quantitative analysis of [^{64}Cu]Cu-NT-CB-DOTA in H1299-tumor–bearing mice at 1, 4, 24, and 48 h after injection. B = bladder; %ID/g = percentage injected dose per gram; T = tumor.

DISCUSSION

To develop novel NTSR-1–targeting radiopharmaceuticals with improved tumor uptake, improved tumor-to-background ratio, and extended tumor residence, we elaborated a strategy to attach MAs to a synthetic antagonistic NTSR-1 ligand. The hypothesis was based on the fact that the net charge around the tracer may be modified by introducing chelators or linker–chelator combinations with several basic nitrogen atoms. Our results showed that the combination of CB-NOTA (linker–chelator) and the bicyclic Sarcage (chelator) directly attached to the neurotensin ligand significantly improved the in vivo PET imaging tumor uptake and tumor-to-background ratio (especially tumor-to-liver ratios) even up to 48 h after injection.

It is worth addressing some future directions of this study. First, our platform showed promising results in the NTSR-1 system. Other target/ligand systems should be used together with CB-NOTA and Sarcage to evaluate the generality of this approach. Second, macrocycles CB-cyclam and Sarcage were the 2 MAs we put to the test. It remains to be seen how other macrocycles may affect these results in terms of size, number of nitrogen atoms, and attachment to the ligand. Third, we were focused on the characterization of **9** because of its ability to chelate multiple radiometals. However, [^{64}Cu]Cu-NT-Sarcage showed increased tumor uptake compared with [^{64}Cu]Cu-NT-CB-NOTA. Fourth, [^{64}Cu]Cu-NT-CB-NOTA and [^{55}Co]Co-NT-CB-NOTA also showed different uptake values in 2 tumor models. Whether the different uptake was caused by the radioisotope or the tumor model needs to be confirmed further. Fifth, in the case of [^{64}Cu]Cu-NT-CB-NOTA and [^{64}Cu]Cu-NT-CB-DOTA, there may be concerns that the ^{64}Cu chelation may have occurred at both the CB-cyclam unit and the chelator. However, CB-cyclam generally requires 90°C heating to form a stable complex with ^{64}Cu during labeling, and it is reasonable to assume that the chelation happened at the NOTA or DOTA locations when heated at 37°C (conditions used in this study). Nonetheless, direct evidence is still needed to confirm this assumption. Sixth, direct comparison with 3BP-227 would have resulted in a better reference to compare with the data obtained from our tracers. Nevertheless, the focus of this research was to improve tumor uptake and retention and to reduce liver uptake. We, therefore, did not compare our agent with 3BP-227 in this research. Finally, the effect of ^{177}Lu with precursors **9** and **10** also remains to be determined, which was not done in this study.

Recently, Garrison et al. used the same synthetic antagonistic NTSR-1–targeting ligand with a different approach to extend the tumor residence time (*43–45*). They proposed a strategy in which low-molecular-weight targeted ligands were attached to irreversible cysteine cathepsin inhibitors. Once the ligand was internalized and transported to the endolysosomal compartments of the cell, the cysteine cathepsin inhibitors (or endolysosomal trapping agents)

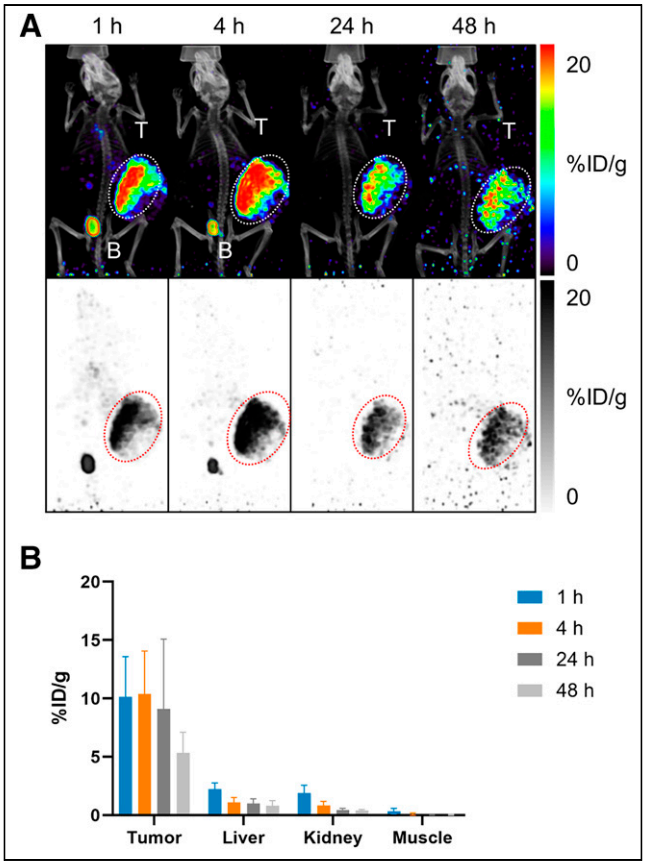

FIGURE 7. (A) Three-dimensional PET/CT images of [^{64}Cu]Cu-NT-Sarcage in H1299-tumor–bearing nu/nu mice at 1, 4, 24, and 48 h after injection. Note that animal-to-animal and tumor size differences were mainly responsible for data spread observed within this group. (B) Quantitative analysis of [^{64}Cu]Cu-NT-Sarcage in H1299-tumor–bearing mice at 1, 4, 24, and 48 h after injection. B = bladder; %ID/g = percentage injected dose per gram; T = tumor.

formed high-molecular-weight irreversible adducts with cysteine proteases. In this way, the receptor-targeted constructs were able to increase tumor retention. In the same study, the impact of charge modification around the cysteine cathepsin inhibitors was also tested in vitro and in vivo using HT29 colon cancer models (*45*). This approach introduced another structural motif to the tracer (cysteine inhibitor), and the construct needed to interact with cysteine proteases. In the future, it would be interesting to perform a side-by-side comparison with our approach that requires the selection of only a chelator or linker–chelator construct and interaction with only 1 target. We also point out that our initial in vivo studies are being conducted using lung and colorectal cancer models to avoid direct competition with Pluvicto. In a follow-up study, it would be interesting to investigate the potential complementary role of NTSR-1–targeted agents alongside Pluvicto in prostate cancer.

CONCLUSION

In this study, we synthesized several new NTSR-1–targeting radiopharmaceuticals based on a nonpeptidic antagonist ligand. Our synthetic rationale was based on the hypothesis that MAs can modulate the net charge around the tracer, which in turn favors its tumor retention through the interaction with the negatively charged external surface of a cell. In this regard, CB-NOTA and Sarcage moieties were found to improve tumor uptake, tumor-to-background ratio, and tumor retention even at 48 h after injection compared with the acyclic 3MA unit. The results of this study suggest that **9** labeled with ^{64}Cu/^{67}Cu, ^{55}Co/^{58m}Co, or ^{68}Ga and **6** labeled with ^{64}Cu/^{67}Cu or ^{55}Co/^{58m}Co may be excellent diagnostic and therapeutic radiopharmaceuticals for NTSR-1–positive cancers that could progress into the clinic. Given the common presence of MAs in drug molecules, it is possible that these MAs could be replaced with CB-NOTA or Sarcage for easy conversion to radiotheranostic agents.

DISCLOSURE

This work was supported in part by the National Science Foundation under grant CHE-1726291 and by National Institutes of Health grants 5R01CA247769, 1R43CA261503, NIH/NCI P01-CA250972, and NCI P30 CA014520. PET/CT imaging was carried out in the UNC Small Animal Imaging Core Facility. The imaging core is supported in part by NIH grant P30-CA016086, and the PET/CT system was funded by NIH grant S10-OD023611. A patent has been filed on intellectual property relating to this work that has been licensed from UNC Chapel Hill to Accunovo Biotech. Zibo Li is one of the cofounders of Accunovo Biotech. No other potential conflict of interest relevant to this article was reported.

ACKNOWLEDGMENTS

We thank the University of North Carolina's Department of Chemistry Mass Spectrometry Core Laboratory, especially Antonio Lazaro Toledo Machin and Brandie Michelle Ehrmann, for their assistance with mass spectrometry analysis. We gratefully acknowledge Justin Jeffery, Ashley Weichmann, and Dr. Zachary Rosenkrans at the University of Wisconsin Carbone Cancer Center for their assistance with animal experiments.

KEY POINTS

QUESTION: Is it possible to develop NTSR-1–targeted radiopharmaceuticals with high tumor uptake, sustained tumor retention, and low background uptake that hold potential for theranostic applications in the clinic?

PERTINENT FINDINGS: With MAs introduced to the NTSR-1 ligand, the resulting agents [^{64}Cu]Cu-NT-CB-NOTA, ^{68}Ga]Ga-NT-CB-NOTA, [^{55}Co]Co-NT-CB-NOTA, and [^{64}Cu]Cu-NT-Sarcage showed high tumor uptake and retention with low background on PET imaging.

IMPLICATIONS FOR PATIENT CARE: This study suggests that leading precursors NT-CB-NOTA and NT-Sarcage are excellent diagnostic and therapeutic candidates as NTSR-1–targeted theranostic agents, which may benefit prostate cancer patients with low PSMA expression.

REFERENCES

1. Annual report to the nation 2022: overall cancer statistics. NIH website. https://seer.cancer.gov/report_to_nation/statistics.html. Updated December 20, 2023. Accessed May 15, 2024.
2. Rebello RJ, Oing C, Knudsen KE, et al. Prostate cancer. *Nat Rev Dis Primers*. 2021;7:9.
3. Posdzich P, Darr C, Hilser T, et al. Metastatic prostate cancer: a review of current treatment options and promising new approaches. *Cancers (Basel)*. 2023;15:461.

4. Malcolm J, Falzone N, Lee BQ, Vallis KA. Targeted radionuclide therapy: new advances for improvement of patient management and response. *Cancers (Basel).* 2019;11:268.
5. FDA approves Pluvicto/Locametz for metastatic castration-resistant prostate cancer. *J Nucl Med.* 2022;63(5):13N.
6. Jadvar H. The VISION forward: recognition and implication of PSMA−/^{18}F-FDG+ mCRPC. *J Nucl Med.* 2022;63:812–815.
7. Cai M, Son XL, Li XA, et al. Current therapy and drug resistance in metastatic castration-resistant prostate cancer. *Drug Resist Updat.* 2023;68:100962.
8. AlSadi R, Bouhali O, Dewji S, Djekidel M. ^{177}Lu-PSMA therapy for metastatic castration-resistant prostate cancer: a mini-review of state-of-the-art. *Oncologist.* 2022;27:e957–e966.
9. Juzeniene A, Stenberg VY, Bruland ØS, Larsen RH. Preclinical and clinical status of PSMA-targeted alpha therapy for metastatic castration-resistant prostate cancer. *Cancers (Basel).* 2021;13:779.
10. Inderjeeth AJ, Iravani A, Subramaniam S, Conduit C, Sandhu S. Novel radionuclide therapy combinations in prostate cancer. *Ther Adv Med Oncol.* 2023;15: 17588359231187202.
11. Sandhu S, Guo C, Hofman MS. Radionuclide therapy in prostate cancer: from standalone to combination PSMA theranostics. *J Nucl Med.* 2021;62:1660–1668.
12. El Fakiri M, Geis NM, Ayada N, Eder M, Eder AC. PSMA-targeting radiopharmaceuticals for prostate cancer therapy: recent developments and future perspectives. *Cancers (Basel).* 2021;13:3967.
13. Falkmer S, Askensten U, Grimelius L, Abrahamsson PA. Cytochemical markers and DNA content of neuroendocrine cells in carcinoma of the prostate gland during tumour progression. *Acta Histochem Suppl.* 1990;38:127–132.
14. Huang J, Wu C, di Sant'Agnese PA, Yao JL, Cheng L, Na Y. Function and molecular mechanisms of neuroendocrine cells in prostate cancer. *Anal Quant Cytol Histol.* 2007;29:128–138.
15. Oesterling JE, Hauzeur CG, Farrow GM. Small cell anaplastic carcinoma of the prostate: a clinical, pathological and immunohistological study of 27 patients. *J Urol.* 1992;147:804–807.
16. Lee LF, Guan J, Qiu Y, Kung HJ. Neuropeptide-induced androgen independence in prostate cancer cells: roles of nonreceptor tyrosine kinases Etk/Bmx, Src, and focal adhesion kinase. *Mol Cell Biol.* 2001;21:8385–8397.
17. Swift SL, Burns JE, Maitland NJ. Altered expression of neurotensin receptors is associated with the differentiation state of prostate cancer. *Cancer Res.* 2010;70:347–356.
18. Amorino GP, Deeble PD, Parsons SJ. Neurotensin stimulates mitogenesis of prostate cancer cells through a novel c-Src/Stat5b pathway. *Oncogene.* 2007;26:745–756.
19. Elek J, Pinzon W, Park KH, Narayanan R. Relevant genomics of neurotensin receptor in cancer. *Anticancer Res.* 2000;20:53–58.
20. Abrahamsson PA, Wadström LB, Alumets J, Falkmer S, Grimelius L. Peptide-hormone- and serotonin-immunoreactive tumour cells in carcinoma of the prostate. *Pathol Res Pract.* 1987;182:298–307.
21. Sehgal I, Powers S, Huntley B, Powis G, Pittelkow M, Maihle NJ. Neurotensin is an autocrine trophic factor stimulated by androgen withdrawal in human prostate cancer. *Proc Natl Acad Sci USA.* 1994;91:4673–4677.
22. Seethalakshmi L, Mitra SP, Dobner PR, Menon M, Carraway RE. Neurotensin receptor expression in prostate cancer cell line and growth effect of NT at physiological concentrations. *Prostate.* 1997;31:183–192.
23. Burkett BJ, Bartlett DJ, McGarrah PW, et al. A review of theranostics: perspectives on emerging approaches and clinical advancements. *Radiol Imaging Cancer.* 2023; 5:e220157.
24. Li M, Wang S, Kong Q, et al. Advances in macrocyclic chelators for positron emission tomography imaging. *VIEW.* 2023;4:20230042.
25. Barrett KE, Houson HA, Lin W, Lapi SE, Engle JW. Production, purification, and applications of a potential theranostic pair: cobalt-55 and cobalt-58m. *Diagnostics (Basel).* 2021;11:1235.
26. Liu S, Li Z, Conti PS. Development of multi-functional chelators based on sarcophagine cages. *Molecules.* 2014;19:4246–4255.
27. Deng H, Wang H, Zhang H, et al. Imaging neurotensin receptor in prostate cancer with ^{64}Cu-labeled neurotensin analogs. *Mol Imaging.* 2017;16:1536012117711369.
28. Iyer MR, Kunos G. Therapeutic approaches targeting the neurotensin receptors. *Expert Opin Ther Pat.* 2021;31:361–386.
29. Maschauer S, Prante O. Radiopharmaceuticals for imaging and endoradiotherapy of neurotensin receptor-positive tumors. *J Labelled Comp Radiopharm.* 2018;61: 309–325.
30. Schulz J, Rohracker M, Stiebler M, et al. Proof of therapeutic efficacy of a ^{177}Lu-labeled neurotensin receptor 1 antagonist in a colon carcinoma xenograft model. *J Nucl Med.* 2017;58:936–941.
31. Baum RP, Singh A, Schuchardt C, et al. ^{177}Lu-3BP-227 for neurotensin receptor 1–targeted therapy of metastatic pancreatic adenocarcinoma: first clinical results. *J Nucl Med.* 2018;59:809–814.
32 . Fusion Pharmaceuticals announces first patient dosed in phase 1 study of FPI-2059, a targeted alpha therapy (TAT) for the treatment of solid tumors expressing NTSR1. Fusion Pharmaceuticals website. https://ir.fusionpharma.com/2023-03-20-Fusion-Pharmaceuticals-Announces-First-Patient-Dosed-in-Phase-1-Study-of-FPI-2059,-a-Targeted-Alpha-Therapy-TAT-for-the-Treatment-of-Solid-Tumors-Expressing-NTSR1. Updated March 20, 2023. Accessed May 15, 2024.
33. Engle JW. The production of Ac-225. *Curr Radiopharm.* 2018;11:173–179.
34. Zhang T, Ma X, Xu M, et al. Chelator boosted tumor-retention and pharmacokinetic properties: development of ^{64}Cu labeled radiopharmaceuticals targeting neurotensin receptor. *Eur J Nucl Med Mol Imaging.* May 21, 2024 (Epub ahead of print].
35. Holik HA, Ibrahim FM, Elaine AA, Putra BD, Achmad A, Kartamihardja AHS. The chemical scaffold of theranostic radiopharmaceuticals: radionuclide, bifunctional chelator, and pharmacokinetics modifying linker. *Molecules.* 2022;27:3062.
36. Metwally S, Stachewicz U. Surface potential and charges impact on cell responses on biomaterials interfaces for medical applications. *Mater Sci Eng C Mater Biol Appl.* 2019;104:109883.
37. Li M, Ma X, Molnar CJ, et al. Modular PET agent construction strategy through strain-promoted double-click reagent with efficient photoclick step. *Bioconjugate Chem.* 2022;33:2088–2096.
38. Lin W, Aluicio-Sarduy E, Houson HA, et al. Theranostic cobalt-55/58m for neurotensin receptor-mediated radiotherapy in vivo: a pilot study with dosimetry. *Nucl Med Biol.* 2023;118:108329.
39. Avila-Rodriguez MA, Nye JA, Nickles RJ. Simultaneous production of high specific activity ^{64}Cu and ^{61}Co with 11.4 MeV protons on enriched ^{64}Ni nuclei. *Appl Radiat Isot.* 2007;65:1115–11120.
40. Lin W, Aluicio-Sarduy E, Barrett KE, et al. Separation of cyclotron-produced cobalt-55/58m from iron targets using cation exchange chromatography with non-aqueous solvents and extraction chromatography. *Appl Radiat Isot.* 2023;200: 110980.
41. Lang C, Gmeiner P. Efficient synthesis of heterocyclic neurotensin receptor ligands by microwave-assisted aminocarbonylation. *Synthesis.* 2013;45:2474–2480.
42. Lin W, Fonseca Cabrera GO, Aluicio-Sarduy E, et al. Radiolabeling diaminosarcophagine with cyclotron-produced cobalt-55 and [^{55}Co]Co-NT-Sarcage as a proof of concept in a murine xenograft model. *Bioconjugate Chem.* 2024;35:412–418.
43. Fan W, Zhang W, Allen S, et al. Examination of charge modifications of an endolysosomal trapping inhibitor in an antagonistic NTSR1-targeted construct for colon cancer. *Bioconjug Chem.* 2022;33:1363–1376.
44. Fan W, Zhang W, Alshehri S, Garrison JC. Examination of the impact molecular charge has on NTSR1-targeted agents incorporated with cysteine protease inhibitors. *Eur J Med Chem.* 2022;234:114241.
45. Fan W, Zhang W, Alshehri S, Neeley TR, Garrison JC. Enhanced tumor retention of NTSR1-targeted agents by employing a hydrophilic cysteine cathepsin inhibitor. *Eur J Med Chem.* 2019;177:386–400.